

Enhanced detectability of axion's electromagnetic response with a RF-excited magnetic field in cavity

Li Gao,^a Hao Zheng,^a Xianing Feng,^a Suirong He,^a Lingbo Zhao,^b Qingquan Jiang,^c
L. F. Wei^a

^a*HgerD Collaboration and Information Quantum Technology Laboratory, School of Information Science and Technology, Southwest Jiaotong University, Chengdu 610031, China.*

^b*School of Science, Donghua University, Shanghai 200051, China*

^c*School of Physics and Astronomy, China West Normal University, Nanchong 637009, China.*

E-mail: lfwei@swjtu.edu.cn

ABSTRACT: Haloscope is one of the typical installations to detect the electromagnetic responses (EMRs) of axion field in radio-frequency (RF) and microwave bands. Given that the detectable signals of the usual Haloscope-type detectors (HTDs), biased only by high stationary magnetic fields, are just the second axion-photon energy and thus are very weak, here we propose a feasible approach to significantly improve their sensitivity by additionally applying a transverse RF- or microwave modulated magnetic field to excite the cavity's magnetic resonant mode to produce the first-order axion-photon energy response signals. Accordingly, it can be argued that the achievable detection sensitivity of the upgrading HTD (i.e., UHTD) **could be enhanced by 3 ~ 4 orders of magnitude**, compared with that achieved by the existing HTDs without the transverse RF-excited magnetic field. The feasibility of the proposed UHTD is also discussed.

ARXIV EPRINT: [2408.16229](https://arxiv.org/abs/2408.16229)

Contents

1	Introduction.	1
2	The signals generated in the HTDs for axion fields detection	3
3	The EM response of the axion field passing through the proposed UHTD	5
4	Significantly improving the achievable detection sensitivity.	9
5	Conclusions and Discussions.	12

1 Introduction.

Dark matter is believed to be one of the indispensable components of the universe, even though it cannot be directly observed [1, 2]. It is believed that the existence of dark matter could be indirectly tested by probing various effects caused by its possible weak interaction with the particles in Standard Model (SM) at the microscopic level [3, 4]. However, up to date, no definitive signal of the dark matter has been discovered yet, although a series of observations have provided various relevant parameter constraints. Given the existence of WIMPs (Weakly Interacting Massive Particles) with larger masses has been ruled out almost completely [5], detections of the lighter dark matter candidates, such as dark photons, axions, and axion-like particles, etc. have received increasing attention in recent years [6].

Roughly, there are three approaches to detect the axions. The first one is the gravitational probes, i.e., searching for the possible signatures in CMB and Pulsar Timing Arrays (PTA) [7–9], for the detection of the axions with exceptionally light masses. Next, the CASPER-type experiments [10, 11] and PandaX-like experiments [12] have been used to

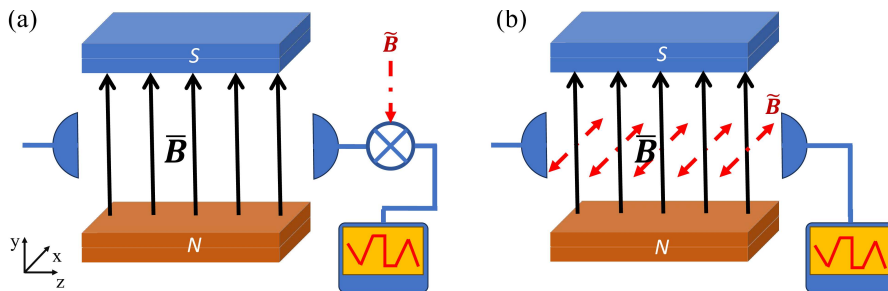


Figure 1. Electromagnetic response detections of axions with a one-dimensional cavity biased by a high stationary magnetic field \vec{B} : (a) The generated EMR signal of the passing axion is coherently amplified ex-situ by applying an additional RF-field; and (b) the EMR signal of the axion is significantly enhanced in-situ, due to the interaction between the excited magnetic mode and the passing axion field.

probe the observable effects induced by the axion-nucleon and axion-electron interactions for the axions with the slightly larger masses. Thirdly, it is believed that the Haloscope-type detectors (HTDs), shown schematically in Figure 1(a) without the radio-frequency (RF) magnetic field $\tilde{B}(t)$ and based on the inverse Primakoff effect [13], are particularly suitable to detect the electromagnetic responses (EMRs) of the axions with μeV -order masses. However, the results obtained by using all the existing HTDs biased only by the high stationary magnetic fields (SMFs), typically including the ADMX [14, 15] and CASTRBF [7, 15, 16], Optical Ring Cavity Technology [17], TOORAD [18], HAYSTAC [19], CAPP [20], ORGAN [21], and TASEH [22] are still null. This implies that the detection sensitivity of these existing HTDs are still expected to be further improved.

Basically, the dark matter axion could be treated as a pseudo-scalar particle in QCD, and its interaction with the electromagnetic field can be described by the following Lagrangian density [23]:

$$\mathcal{L} = F_{\mu\nu}F^{\mu\nu} + j_\mu A^\mu - \frac{1}{2}m_a^2 a^2 + \frac{1}{2}\partial_\mu a \partial^\mu a - g_{a\gamma\gamma} a F_{\mu\nu} \tilde{F}^{\mu\nu}, \quad (1.1)$$

here, j_μ denotes the usual four-current density, A^μ stands for the electromagnetic four-potential, $F_{\mu\nu}$ and $\tilde{F}_{\mu\nu}$ are the electromagnetic field tensor and its dual, respectively. Here, a is the axion field with the mass m_a and the oscillation frequency $\omega_a = m_a c^2 / \hbar$. Here, c is the speed of light and \hbar the reduced Planck constant. Usually, the decay parameter f_a of the axion can be described as $f_a = 10^{12} \text{GeV}$, and $g_{a\gamma\gamma} = g_\gamma f_a^{-1} \alpha / \pi$ is the axion-photon coupling strength, with α being the fine-structure constant and g_γ a dimensionless constant depending on the axion models. Specifically, $g_\gamma = -0.97$ in the KSVZ model [24, 25], and $g_\gamma = 0.36$ in the DFSZ one [26, 27]. Generically, the achievable minimum value of $g_{a\gamma\gamma}$ refers to the detection sensitivity of the axion field.

In principle, by further enhancing the strength of the applied SMF, the detection sensitivity of the existing HTD can be further improved. However, its feasibility is limited both technologically and financially. Therefore, an improved approach shown schematically in Figure 1(a) could be utilized to 'ex-situ' coherently amplify the EMR signal $S_{a\rightarrow\gamma}^C(t)$ generated in the usual HTDs [28–31], by coherently mixing the additionally applied RF-frequency signal $\tilde{B}(t)$ with the original signal $S_{a\rightarrow\gamma}^C(t)$. This approach has certainly improved the detectability of $S_{a\rightarrow\gamma}^C(t)$, which can be coherently amplified as $P_1(t)$ now. But additional noise is introduced simultaneously by the application of $\tilde{B}(t)$. Consequently, the achievable detection sensitivity remains still very limited, at least theoretically.

Alternatively, in the present work we propose a conceptually novel approach, see Figure 1(b) for simple comparison, to upgrade the existing HTD configuration (hereafter referred to as UHTD), i.e., keeping the longitudinal high SMF unchanged but additionally just apply a weak transverse RF-excited magnetic field $\tilde{B}(t)$ to excite the cavity's magnetic resonant mode for in-situ enhancing the axion-photon interference energy. As a consequence, the power of the generated EMR signal $S_{\text{rf}}^{(1)}(t)$ is now proportional to the axion-photon coupling strength, unlike in the existing HTD wherein the EMR signal $S_{a\rightarrow\gamma}^C(t)$ is just proportional to the square of the axion-photon coupling strength.

Given the transverse RF-excited field technique has been widely applied in the magnetic resonance imagings, various filtering- and heat conduction techniques, it is argued

that the achievable detection sensitivity of the UHTD for the EMR detection of axion field in RF-band could be enhanced by $3 \sim 4$ orders of magnitude compared with the existing HTDs. Therefore, it is expected that the proposed UHTD might greatly push the progress for the Haloscope detection of axion field in RF-band.

The paper is arranged as follows. In Sec. 2 we first review briefly how the axion fields can be detected with the existing HTDs and then discuss the limitation in the previous approaches by additionally applying the RF signals to ex-situ coherently amplify the original EMR signals for improving their sensitivity. In Sec. 3, we demonstrate how the axion-photon interference energy can be significantly enhanced in the UHTD. In Sec. 4, we specifically investigate the achievable detection sensitivity by probing the first-order electromagnetic response signal generated in the UHTD, and we evaluate the noise effective power of the UHTD through a rigorous noise analysis. Finally, in Sec. 5, we summarize our work and discuss the feasibility of the proposed UHTD.

2 The signals generated in the HTDs for axion fields detection

In this section we first review briefly how the axion fields can be detected with the existing HTDs and then discuss the limitation in the previous approaches by additionally applying the rf signals to ex-situ coherently amplify the original EMR signals for improving their sensitivity. It is well-known that, in the usual HTD, which is biased by a high stationary magnetic field $\mathbf{B}^{(0)}$, the axion-modified Maxwell equation [23]:

$$\begin{cases} \nabla \cdot \mathbf{E}(t) = \frac{1}{\varepsilon_0} g_{a\gamma\gamma} \mathbf{B}^{(0)} \cdot \nabla a, \\ \nabla \times \mathbf{B}(t) - \frac{1}{c^2} \partial_t \mathbf{E}(t) = -\mu_0 g_{a\gamma\gamma} \mathbf{B}^{(0)} \partial_t a, \end{cases} \quad (2.1)$$

can be obtained from the Lagrangian Eq. (1.1). Here, $a = a(\mathbf{x}, t)$ is the axion field, ε_0 is permittivity and μ_0 the permeability in vacuum; $\mathbf{B}(t)$ and $\mathbf{E}(t)$ are the magnetic- and electric field densities of the EMR signal generated in the HTD, respectively. Without the axion field and neglecting the background EM noise, the electromagnetic field in the HTD cavity can be expressed as $E(t=0) = 0$ and $B(t=0) = B^{(0)}$. Now, if an axion field passes through the HTD's cavity, an EMR signal with $E(t > 0) \neq 0$ and $B(t > 0) > B^{(0)}$ can be generated for the detection.

Specifically, when an approximately isotropic axion wave, i.e., $\nabla a \ll \partial_t a$ and thus $a(\mathbf{x}, t) = \text{Re}(a_0 e^{-i(\omega_a t + \phi_a)})$ (with ϕ_a being the random phase within the range $[0, 2\pi)$ [32, 33]) and $\rho_{\text{eff}} \sim 0$, passes through a cavity biased by a high SMF $\mathbf{B}^{(0)} = \bar{B}(\mathbf{x})$ (which is assumed to be along the y -direction), then an effective current:

$$\mathbf{j}_{\text{eff}}(\mathbf{x}, t) = -g_{a\gamma\gamma} \bar{B}(\mathbf{x}) \partial_t a, \quad (2.2)$$

it satisfies the following dynamical equation:

$$\left(\frac{d^2}{dt^2} + \Gamma_l \frac{d}{dt} + \omega_l^2 \right) \psi_l(t) = \mu_0 \mathbf{j}_{\text{eff}}(\mathbf{x}, t), \quad (2.3)$$

where $\Gamma_l = \omega_l/Q_l$ is the energy dissipation rate of the l -th mode with $Q_l = \omega_l/\Gamma_l$ being its quality factor. By solving (2.3), the response electromagnetic field induced by the axion can be obtained.

Above, we assume that the response is resonant, i.e., $\omega_a = \omega_l$, and the experimental parameters are set typically as [27]: $g_\gamma = 0.36$, $\rho_a = 2^{-1} \times 10^{-24}$ g/cm³, $\bar{B} = 8$ T, $V = 1$ m³, $Q_l = 10^4$, $\omega_a = 2\pi \times 1$ GHz, and $f_a m_a = 6 \times 10^{15}$ (eV)², the response electric field is $|\bar{E}_y^{(1)}| = 1.0095 \times 10^{-10}$ (V/m), and the magnetic field is $|\bar{B}_x^{(1)}| = 3.365 \times 10^{-17}$ T. Obviously, both the electric- and magnetic field intensities of the response signals of the passing axion field, generated in the usual HTD, are virtually undetectable; even with the most sensitive electric [34, 35] and magnetic field detectors [36] available today, they are still a few orders of magnitude away from the sensitivities required to effectively probe these significantly weak signals. Therefore, the energy detection of the electromagnetic response signal of the passing axion field is necessary.

The detectable power of the axion response signal in the HTDs, for the resonant response with $\omega_l = \omega_a$, can be expressed as:

$$P_{a \rightarrow \gamma}^{(2)} = g_{a\gamma\gamma}^2 \times \frac{2\rho_a \omega_a}{m_a^2 \mu_0} \bar{B}^2 Q_l C_l V, \quad (2.4)$$

with $C_l = (\int_V d^3x \bar{B}(\mathbf{x}) \cdot \mathbf{e}_l(\mathbf{x}))^2 / (\bar{B}^2 V)$ being the form factor of the l -th mode of the electromagnetic field. [The relevant derivation is provided in Appendix A.](#) Currently, most axion detection devices are based on this theory, in which the detectable signal is proportional to the square of the extremely small coupling parameter $g_{a\gamma\gamma}$. This explains why all experimental searches using HTDs have so far yielded no positive results. Therefore, upgrading the usual HTD-type installations to further improve their achievable detection sensitivities for capturing the weaker electromagnetic response signals of the axion fields, corresponding to the smaller axion-photon coupling parameter $g_{a\gamma\gamma}$, is particularly desirable.

Therefore, to enhance its detectability, one must either continue to increase the strength of the steady-state strong magnetic field \bar{B} for generating the stronger electromagnetic response signal (as Eq. (2.4) shows that the power of such an EMRs is proportional to increase the strength of SMF \bar{B}), or coherently amplify the amplitude of the generated electromagnetic response signal for improving its detectability. To overcome the limitations of the former approach, which is constrained by the high manufacturing cost of the steady-state magnetic field, Ref. [30] proposed a novel method: injecting photons into the system and using a power detector to measure the variance of the interference signal from axions. However, the detected signal in Ref. [30] remains the traditional HTDs second-order axion power signal $P_{\text{rf}}^{(2)} \propto g_{a\gamma\gamma}^2$. By injecting intense photons, the weak axion signal is expected to be amplified as measurable variance $\hat{\sigma}^2(N_T) = N_s + \text{others}$ (where $N_s \propto g_{a\gamma\gamma}^2$), and the axion response signal power should be greater than 10^{-6} mW. However, for extremely weak axion-photon coupling, generating such a strong axion signal remains highly challenging (see Appendix B for details) [30].

3 The EM response of the axion field passing through the proposed UHTD

In this section, we demonstrate how the axion-photon energy transferring rate can be significantly enhanced in the UHTD, whose principle has been described briefly in Sec. 1. Differing from the external coherent amplification of the responded signal mentioned above, which is merely aimed at improving its detectability, the additionally applied RF- field applied here is used to excite the cavity's magnetic resonant mode to significantly enhancing the axion-photon converted rate for generating the significantly detectable signals.

Now, let us consider a simplified configuration, shown in Figure 1(b), to upgrade the existing HTDs for the sensitive EMR detection of the axion. Besides the usual high SMF \bar{B} applied along the y -direction, a RF-excited field is applied here to excite the cavity's magnetic resonant mode along the x - direction with the amplitude being $\tilde{B} \ll \bar{B}$. As a consequence, the background magnetic field in the existing HTD can be upgraded as:

$$\mathbf{B}^{(0)}(\mathbf{x}, t) = \bar{B}\mathbf{e}_y + \tilde{B}\text{Re}\left(e^{i(\mathbf{k}_B \cdot \mathbf{x} - \omega_B t)}\right)\mathbf{e}_x, \quad (3.1)$$

where \tilde{B} , \mathbf{k}_B and ω_B is the amplitude, wave vector and frequency of the RF-excited field, respectively. Taking the background magnetic field Eq. (3.1) into the axion-modified Maxwell equations shown in Eq. (2.1), the equations solution can be formally expressed as:

$$\begin{cases} \mathbf{B} = \mathbf{B}^{(0)} + \mathbf{B}^{(1)} + \mathcal{O}^{(2)}(g_{a\gamma\gamma}), \\ \mathbf{E} = \mathbf{E}^{(0)} + \mathbf{E}^{(1)} + \mathcal{O}^{(2)}(g_{a\gamma\gamma}), \end{cases} \quad (3.2)$$

the superscripts: (0) and (1), indicate the effects related to the zeroth- and first-order (1st) responses of the axion-photon coupling, and the effects related to the second-order (2nd) and higher ones, i.e., $\mathcal{O}^{(2)}$, are safely neglected.

Given the zeroth-order effect can be easily calculated by solving the conventional Maxwell equation in the absence of axion-photon coupling. The 1st EMR of the axion can be described by

$$\begin{cases} \nabla \cdot \mathbf{E}^{(1)} = \frac{1}{\varepsilon_0} g_{a\gamma\gamma} \mathbf{B}^{(0)} \cdot \nabla a \sim 0, \\ \nabla \mathbf{B}^{(1)} - \frac{1}{c^2} \partial_t \mathbf{E}^{(1)} = \mu_0 \mathbf{j}_{\text{eff}}^{(1)}(\mathbf{x}, t), \end{cases} \quad (3.3)$$

for the approximately isotropic axion wave, i.e., the axion field can be described as $a(\mathbf{x}, t) \approx \text{Re}(a_0 e^{-i(\omega_a t + \phi_a)})$.

Under the Lorenz gauge condition; where $\mathbf{B}^{(1)} = \nabla \times \mathbf{A}^{(1)}$, $\mathbf{E}^{(1)} = -\partial_t \mathbf{A}^{(1)} - \nabla \phi^{(1)}$, $\nabla \cdot \mathbf{A}^{(1)} + \partial_t \phi^{(1)} = 0$, we can conclude that: $-\nabla^2 \mathbf{A}^{(1)} + \partial_t^2 \mathbf{A}^{(1)}/c^2 = \mathbf{j}_{\text{eff}}^{(1)}$, When a RF-excited magnetic field is added perpendicular to the direction of the steady magnetic field, the resulting axion response effective current will become

$$\mathbf{j}_{\text{eff}}^{(1)} = -\frac{1}{4c} g_{a\gamma\gamma} [\bar{B}\mathbf{e}_y + \tilde{B}\text{Re}(e^{i(\mathbf{k}_B \cdot \mathbf{x} - \omega_B t)})\mathbf{e}_x] \times \partial_t a. \quad (3.4)$$

In the cavity, the electromagnetic vector potential $\mathbf{A}^{(1)}$ can be expanded in terms of a series of discrete modes: $\mathbf{A}^{(1)} = \sum_l \mathbf{u}_l(\mathbf{x})\psi_l(t)$. For the l -th cavity mode with the

dissipation Γ_l , its response to the axion field, i.e., the signal transported along the x -direction can be divided into space part and time-dependent part. And the space part satisfies the orthogonality, normalization, and completeness relations. Then, the time-dependent part will satisfy the following equation:

$$\left(\frac{d^2}{dt^2} + \Gamma_l \frac{d}{dt} + \omega_l^2\right)\psi_{x,l}^{(1)}(t) = a_{lx}\Omega \text{Re}(e^{-i(\omega_a t + \phi_a)}) \text{Re}(e^{-i\omega_B t}), \quad (3.5)$$

with $\Omega = cg_{a\gamma\gamma}\omega_a|a_0|/4$ and $a_{lx} = \int_V \tilde{B}(\mathbf{x}) \cdot \mathbf{u}_l^*(\mathbf{x}) d^3x$ is the overlap coefficient of the effective flow to cavity mode. The electromagnetic vector potential x -component solution reads $\mathbf{A}_{x,l}^{(1)}(\mathbf{x}, t) = \left(A_{x,l+}^{(1)}(\mathbf{x}, t) + A_{x,l-}^{(1)}(\mathbf{x}, t)\right) \mathbf{e}_x$, where $A_{x,l\pm}^{(1)}(\mathbf{x}, t) = \text{Re}[ia_{lx}\Omega \mathbf{u}_l(\mathbf{x}) e^{-i(\Delta_{aB}^\pm t + \phi_a)} / (\omega_l^2 - (\Delta_{aB}^\pm)^2 - i\Gamma_l(\Delta_{aB}^\pm))]$, and $\Delta_{aB}^\pm = \omega_a \pm \omega_B$. Similarly, for the response along the y -direction, we have

$$\left(\frac{d^2}{dt^2} + \Gamma_l \frac{d}{dt} + \omega_l^2\right)\psi_{y,l}^{(1)}(t) = a_{ly}\Omega \text{Re}(e^{-i(\omega_a t + \phi_a)}), \quad (3.6)$$

where, $a_{ly} = \int_V \tilde{B}(\mathbf{x}) \cdot \mathbf{u}_l^*(\mathbf{x}) d^3x$, whose solution reads $\mathbf{A}_{y,l}^{(1)}(\mathbf{x}, t) = a_{ly}\Omega \mathbf{u}_l(\mathbf{x}) \text{Re}[ie^{-i(\omega_a t + \phi_a)} / (\omega_l^2 - \omega_a^2 - i\Gamma_l\omega_a)] \mathbf{e}_y$. According to the relationship between electromagnetic field and the magnetic vector potential, the electromagnetic Eq. (3.2) in the cavity can be specifically expressed as:

$$\begin{cases} \mathbf{E} = \tilde{E}_x^{(1)} \mathbf{e}_x + [E_y^{(0)} + \bar{E}_y^{(1)}] \mathbf{e}_y, \\ \mathbf{B} = [\tilde{B}_x^{(0)} + \bar{B}_x^{(1)}] \mathbf{e}_x + [\bar{B} + \tilde{B}_y^{(1)}] \mathbf{e}_y, \end{cases} \quad (3.7)$$

with

$$\begin{cases} \mathbf{E}_y^{(0)}(\mathbf{x}, t) = -\text{Re}(c\tilde{B}e^{i(\mathbf{k}_B \cdot \mathbf{x} - \omega_B t)}) \mathbf{e}_y, \\ \mathbf{B}^{(0)}(\mathbf{x}, t) = \bar{\mathbf{B}} \mathbf{e}_y + \text{Re}(\tilde{B}e^{i(\mathbf{k}_B \cdot \mathbf{x} - \omega_B t)}) \mathbf{e}_x, \end{cases} \quad (3.8)$$

for the zeroth-order EMR signal,

$$\begin{cases} \tilde{E}_x^{(1)}(\mathbf{x}, t) = a_{lx}\Omega \mathbf{u}_l(\mathbf{x}) (\Delta_{aB}^+ \Phi_{l+} + \Delta_{aB}^- \Phi_{l-}), \\ \bar{E}_y^{(1)}(\mathbf{x}, t) = \omega_a a_{ly} \Omega \mathbf{u}_l(\mathbf{x}) \Phi_l, \end{cases} \quad (3.9)$$

and

$$\begin{cases} \tilde{B}_y^{(1)}(\mathbf{x}, t) = -\mathbf{k}_l a_{lx} \Omega \mathbf{u}_l(\mathbf{x}) [\Phi_{l+} + \Phi_{l-}], \\ \bar{B}_x^{(1)}(\mathbf{x}, t) = -\mathbf{k}_l a_{ly} \Omega \mathbf{u}_l(\mathbf{x}) \Phi_l, \end{cases} \quad (3.10)$$

for the 1st EMR signal. Above, $\Phi_{l\pm} = \text{Re}\left(e^{-i(\Delta_{aB}^\pm t + \phi_a)} / [\omega_l^2 - (\Delta_{aB}^\pm)^2 - i\Gamma_l(\Delta_{aB}^\pm)]\right)$, $\Phi_l = \text{Re}\left(e^{-i(\omega_a t + \phi_a)} / [\omega_l^2 - \omega_a^2 - i\Gamma_l\omega_a]\right)$, and $\mathbf{k}_l = \omega_l/c$. Obviously, these intensities are proportional to the weak axion-photon coupling strength $g_{a\gamma\gamma}$. **Alongside the original Haloscope response fields $\bar{E}_y^{(1)}$ and $\bar{B}_x^{(1)}$, the RF-excited magnetic field induces an additional first-order axion-converted response, $\tilde{E}_x^{(1)}$ and $\tilde{B}_y^{(1)}$. Consequently, the axion-response electric field is enhanced from $|\bar{E}_y^{(1)}|$ to $(|\bar{E}_y^{(1)}|^2 + |\tilde{E}_x^{(1)}|^2)^{1/2}$. In Figure 2, we shows schematically such a weak contribution from the axion-photon energy conversion brought by the transverse RF-excited field. While, with such a RF-excited magnetic field driving, the 1st**

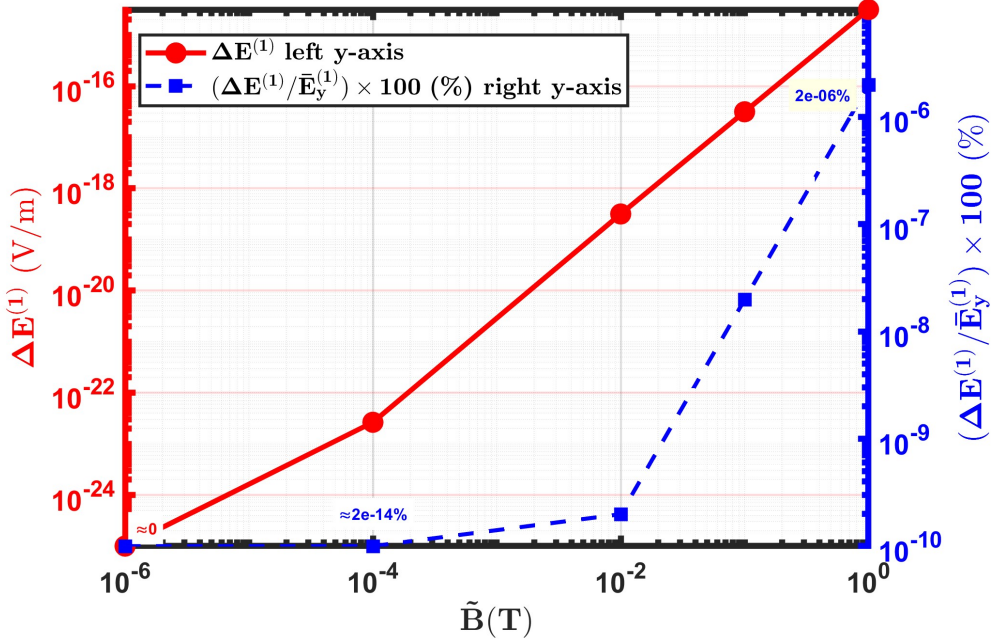


Figure 2. The increment and relative percentage increment of the 1st-order axion-induced electric field induced by the RF-excited magnetic field.

interference energy flux density of the axion response signal can be additionally generated as:

$$\begin{aligned}
\mathbf{S}_{\text{rf}}^{(1)} &= \frac{1}{\mu_0} \left(\tilde{E}_x^{(1)} \bar{B} - E_y^{(0)} \bar{B}_x^{(1)} - \bar{E}_y^{(1)} B_x^{(0)} \right) \mathbf{e}_z \\
&= -\frac{1}{\mu_0} a_{lx} \Omega \bar{B} \mathbf{u}_l(\mathbf{x}) [\Delta_{aB}^+ \Phi_{l+} + \Delta_{aB}^- \Phi_{l-}] \mathbf{e}_z + \frac{\omega_l}{\mu_0} a_{ly} \Omega \mathbf{u}_l(\mathbf{x}) \tilde{B} \Phi_l \text{Re} \left(e^{i(\mathbf{k}_B \cdot \mathbf{x} - \omega_B t)} \right) \mathbf{e}_z,
\end{aligned} \tag{3.11}$$

besides the zeroth-order energy flux, $\mathbf{S}_{\text{rf}}^{(0)} = E_y^{(0)} B_x^{(0)} \mathbf{e}_z / \mu_0$ (shown in Eq. (3.8)), which is independent of axion.

Continuously, the 2nd energy flux density of the present EMR signal of the axion field can be calculated as:

$$\begin{aligned}
\mathbf{S}_{\text{rf}}^{(2)} &= \frac{\Gamma_l}{\mu_0} \mathbf{E}^{(1)} \times \mathbf{B}^{(1)} = \frac{\Gamma_l}{\mu_0} \left(\tilde{E}_x^{(1)} \tilde{B}_y^{(1)} - \bar{E}_y^{(1)} \bar{B}_x^{(1)} \right) = \frac{\Gamma_l}{\mu_0} \left(\partial_t A_{x,l}^{(1)} \partial_z A_{x,l}^{(1)} + \partial_t A_{y,l}^{(1)} \partial_z A_{y,l}^{(1)} \right) \\
&= -\frac{\Gamma_l}{\mu_0} \mathbf{k}_l a_{lx}^2 \Omega^2 \mathbf{u}_l^2(\mathbf{x}) [(\Delta_{aB}^+ \Phi_+ + \Delta_{aB}^- \Phi_{l-})(\Phi_+ + \Phi_{l-})] + \frac{\Gamma_l}{\mu_0} \mathbf{k}_l \omega_a a_{ly}^2 \Omega^2 \mathbf{u}_l^2(\mathbf{x}) \Phi_l^2,
\end{aligned} \tag{3.12}$$

and its time-average reads

$$\langle \mathbf{S}_{\text{rf}}^{(2)} \rangle = c g_{a\gamma\gamma}^2 |a_0|^2 \omega_a Q_l (\bar{B}^2 + \tilde{B}^2) C_l V \mathbf{e}_z, \tag{3.13}$$

which is obviously proportional to the square of axion-photon coupling strength (as $\Omega = c g_{a\gamma\gamma} \omega_a |a_0| / 4$ defined in Eq. (3.5)), the squares of amplitudes of the biased high SMF (as

$a_{ly} \sim \bar{B}$ shown in Eq. (3.6)), and the additionally applied RF-excited field (as $a_{lx} \sim \tilde{B}$ shown in Eq. (3.5)). Since $\bar{B} \gg \tilde{B}$, the 2nd energy response is mainly contributed by the biased high SMF. In contrast, the 1st interference energy flux density response of the passing axion field is only generated by the applied RF-excited field, i.e., for $\tilde{B} = 0$ and thus $a_{lx} = 0$, we have $S_{\text{rf}}^{(1)} = 0$.

Physically, the phase factor might be treated as an arbitrarily unknown random variable, and thus if it influences the axion-photon energy conversion should be discussed. Following Refs. [32, 33], the 1st interference energy flux density of the axion's response signal, shown in Eq. (3.11) for $\phi_a = 0$, should be replaced as the ϕ_a -dependent one $S_{\text{rf}}^{(1)}(\phi_a)$. Consequently, under the resonant driving, i.e., $\omega_a = \omega_B = \omega_l$, the time-average of $S_{\text{rf}}^{(1)}$ should be expressed as [32, 33],

$$\begin{aligned} \langle S_{\text{rf}}^{(1)}(\phi_a) \rangle &= \lim_{T \rightarrow \infty} \frac{1}{T} \int_0^T \frac{e_z}{\mu_0} \left(\tilde{E}_x^{(1)} \bar{B} - E_y^{(0)} \bar{B}_x^{(1)} - \bar{E}_y^{(1)} B_x^{(0)} \right) dt \\ &= cg_{a\gamma\gamma} |a_0| \bar{B} \tilde{B} Q_l C_l V \cos(\phi_a) e_z. \end{aligned} \quad (3.14)$$

where $C_l = (\int_V d^3x \bar{B}(\mathbf{x}) \cdot \mathbf{u}_l(\mathbf{x}) \int_V d^3x \tilde{B}(\mathbf{x}) \cdot \mathbf{u}_l(\mathbf{x})) / (\bar{B} \tilde{B} V)$ is the form factor of the l -th mode electromagnetic field in the cavity. By making the statistical average on the random phase, we have

$$\overline{\langle S_{\text{rf}}^{(1)}(\phi_a) \rangle} = cg_{a\gamma\gamma} |a_0| \bar{B} \tilde{B} Q_l C_l V \overline{\cos(\phi_a)} e_z, \quad (3.15)$$

where $\overline{\cos(\phi_a)}$ is the statistical average of $\cos(\phi_a)$ for the unknown stochastic phase $\phi_a \sim [0, 2\pi)$ [32, 33]. As a result, it cannot be directly detected, as $\overline{\cos(\phi_a)}$ is zero for the long-time averages.

Alternatively, we show below that the stable output of 1st-order axion response signals can be implemented by using the usual IQ-mixer modulation technique, although the phase of the 1st-order axion response signal is still random [37–39]. In fact, the 1st interference energy flux density shown in Eq. (3.11) can be rewritten as:

$$S_{\text{rf}}^{(1)}(t) = |S_{\text{rf}}^{(1)}| [\cos(\Delta_{aB}^+ t + \phi_a) + \cos(\Delta_{aB}^- t + \phi_a)], \quad (3.16)$$

with $|S_{\text{rf}}^{(1)}| = ca_0 g_{a\gamma\gamma} \omega_a^2 \bar{B} \tilde{B} / (4\mu_0 \Gamma \omega_a)$ being its amplitude. Under the resonant condition, i.e., $\omega_a = \omega_B = \omega_l$, we have $S^{(1)}(t) \sim |S_{\text{rf}}^{(1)}| [\cos(2\omega_B t + \phi_a) + \cos(\phi_a)]$, which can be split into two signals $S_1^{(1)}(t)$ and $S_2^{(1)}(t)$ with the same amplitude of $|S_{\text{rf}}^{(1)}|/2$. They are mixed with the local coherent electromagnetic signals $L_1(t) \sim L \cos(2\omega_B t)/2$ and $L_2(t) \sim L \sin(2\omega_B t)/2$. After the low-pass filtering, we get the $I(\phi_a)$ -channel signal: $I(\phi_a) = \frac{1}{4} |S_{\text{rf}}^{(1)}| L \cos(\phi_a)$, and the $Q(\phi_a)$ -channel signal: $Q(\phi_a) = -\frac{1}{4} |S_{\text{rf}}^{(1)}| L \sin(\phi_a)$, respectively. Finally, the amplitude of the 1st interference energy flux density amplitude $|S_{\text{rf}}^{(1)}|$, can be determined by the demodulation signal with the usual IQ mixer technique, i.e.,

$$D = \sqrt{I^2(\phi_a) + Q^2(\phi_a)} = \frac{1}{4} |S_{\text{rf}}^{(1)}| L, \quad (3.17)$$

which is proportional to $g_{a\gamma\gamma}$ and independent of the signal phase (see Appendix C for details). The next question is, if such a first-order power signal could be detected at a sufficiently sensitive level.

4 Significantly improving the achievable detection sensitivity.

In this section, we discuss the achievable detection sensitivity of axion field by probing the first-order power signal amplitude $P_{\text{rf}}^{(1)}$. Physically, the energy flux density of signal in the cavity can be effectively divided into the zeroth-order response power, the 1st-order response power, and also the second-order one. Basically, the zeroth-order component can be removed via differential filtering, while the 2nd-order component, equivalent to the detection power of a conventional HTDs, is exceedingly weak and thus offers minimal detectability. Therefore, it is expected to extract the amplitude of the 1st-order interference energy flux density.

With the detector area $\Delta S = 1 \text{ mm}^2$ determined, the 1st-order response power is given by:

$$P_{\text{rf}}^{(1)} = \frac{1}{2\mu_0} c g_{a\gamma\gamma} |a_0| \tilde{B} \bar{B} Q_l C_l V. \quad (4.1)$$

The excited magnetic field \tilde{B} in the 1st-order signal power is not an ideal signal. By using the usual noise transfer formula, its uncertainty can be expressed as

$$\Delta P_{\text{rf}}^{(1)} = \frac{\partial P_{\text{rf}}^{(1)}}{\partial \tilde{B}} \Delta \tilde{B} + \frac{\partial P_{\text{rf}}^{(1)}}{\partial \bar{E}_y^{(1)}} \Delta \bar{E}_y^{(1)} = \Delta P_{\tilde{B}}^{(1)} + \Delta P_{\bar{E}_y^{(1)}}^{(1)}, \quad (4.2)$$

with $\tau = 10^{-6} \text{ s}$ ($\tau \leq \tau_a$) being the detection duration, and $\Delta \tilde{B} = (\mu_0 \hbar \omega_0 / (2c \Delta S \tau))^{1/2}$, $\partial P_{\text{rf}}^{(1)} / \partial \bar{E}_y^{(1)} = \tilde{B} \Delta S / (2\mu_0)$, $\Delta \bar{E}_y^{(1)} = (\hbar \omega_a / (2\varepsilon_0 V \Gamma_l \tau))^{1/2}$. Additionally, for the signal with the average photon number $\bar{N} = P_{\text{rf}}^{(1)} \tau / \hbar \omega_a$, its shot noise power over the detection time τ could be calculated as $P_{\text{Shot}} = (P_{\text{rf}}^{(1)} \hbar \omega / \tau)^{1/2}$. Moreover, the equivalent noise temperature originating from the cavity temperature and the transmission chain (i.e., the mixer and the IF-chain) is equivalent to a noise temperature T_{sys} , and the corresponding thermal noise power is given by: $P_{\text{T}} = \hbar \omega [1/2 + (\exp(\hbar \omega / k_B T_{\text{sys}}) - 1)^{-1}] \Delta f$ with $\Delta f = 20 \text{ Hz}$ being the detection bandwidth. Consequently, the signal-to-noise ratio (SNR) of the target signal can be expressed as:

$$\text{SNR} = \frac{P_{\text{rf}}^{(1)} \sqrt{t_{\text{in}} \Delta f}}{\Delta P_{\text{rf}}^{(1)} + P_{\text{Shot}} + P_{\text{T}}}, \quad (4.3)$$

where $t_{\text{in}} = 20 \text{ s}$ is the integration time [40]. With the detectable condition with $\text{SNR} \geq 1$, we get the achievable detection sensitivity:

$$g_{a\gamma\gamma}^{(1)} \geq \left[\frac{\sqrt{\frac{\kappa_1 \hbar \omega_a}{\tau}} + \sqrt{\frac{\kappa_1 \hbar \omega_a}{\tau} + 4(\kappa_1 - \frac{\kappa_1}{\tilde{B}} \Delta \tilde{B})(P_{\text{T}} + \Delta P_{\bar{E}_y^{(1)}}^{(1)})}}{2(\kappa_1 \sqrt{t_{\text{in}} \Delta f} - \frac{\kappa_1}{\tilde{B}} \Delta \tilde{B})} \right]^2, \quad (4.4)$$

with $\kappa_1 = P_{\text{rf}}^{(1)} / g_{a\gamma\gamma}$. For comparison, the 2nd-order response power:

$$P_{\text{C}}^{(2)} = \frac{1}{2\mu_0} g_{a\gamma\gamma}^2 |a_0|^2 \omega_a Q_l (\bar{B}^2 + \tilde{B}^2) C_l V. \quad (4.5)$$

reduces to that obtained by the usual HTDs, wherein the noises are primarily governed by the shot- and thermal noises. Similarly, the SNR for the usual 2nd-order power can be expressed as:

$$\text{SNR} = \frac{P_C^{(2)} \sqrt{t_{in} \Delta f}}{P_{\text{shot}} + P_T}, \quad (4.6)$$

where $P_{\text{shot}} = (P_C^{(2)} \hbar \omega_a / \tau)^{1/2}$. Again, with the detectable condition with $\text{SNR} \geq 1$, the constraint on the axion coupling constant $g_{a\gamma\gamma}$ reads:

$$g_{a\gamma\gamma}^{(2)} \geq \frac{1}{2\kappa_2 \sqrt{t_{in} \Delta f}} \left(\sqrt{\frac{\kappa_2 \hbar \omega_a}{\tau}} + \sqrt{\frac{\kappa_2 \hbar \omega_a}{\tau} + 4\kappa_2 P_T} \right), \quad (4.7)$$

where $\kappa_2 = P_C^{(2)} / g_{a\gamma\gamma}^2$.

Figure 3 illustrates the achievable detection sensitivity limits for the upgraded detection scheme proposed here and the usual HTDs. Specifically, the red and black lines correspond to the sensitivity curves predicted by the KSVZ [24, 25] and DFSZ models [26, 27], respectively. It is clearly seen that, for conventional second-order response power signal

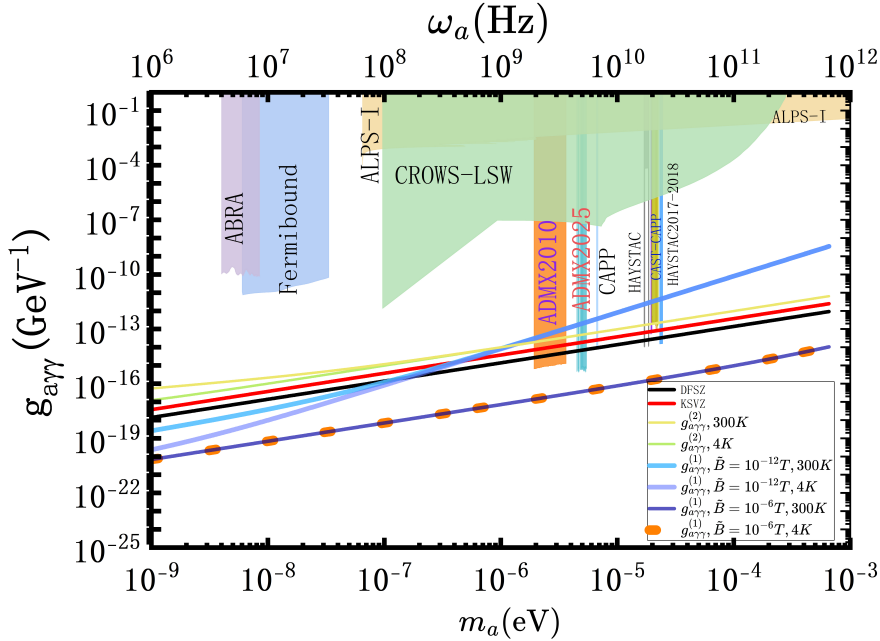


Figure 3. Sensitivity comparison of axion electromagnetic response detection of different masses in microwave cavity with strong magnetic field. In the figure, $g_{a\gamma\gamma}^{(1)}$ and $g_{a\gamma\gamma}^{(2)}$ represent the corresponding sensitivity parameters of the first order (with RF field driven) and second order (without RF field drive) energy response signal detection, respectively. Black and red represent the expected sensitivity of the DFSZ model and the KSVZ model, respectively; The area covered by various colors indicates the sensitivity achieved by the corresponding experiment.

detection, the achievable detection sensitivity is predominantly limited by thermal noise in

the low-frequency region (MHz–100 MHz). Specifically, the detection sensitivity improves as the temperature decreases. Conversely, in the high-frequency region (100 MHz–100 GHz), shot noise constitutes the dominant limitation on the achievable detection sensitivity. In contrast, for the first-order response sensitivity, provided the RF-excited field amplitude is sufficiently large e.g., $\tilde{B} \geq 10^{-6}\text{T}$, the detrimental effects of thermal noise can be effectively suppressed, thereby making an exceptionally high detection sensitivity achievable even at room temperature.

Interestingly, based on our calculation, under the extremely low-temperature conditions, the detection sensitivity of conventional HTDs, with the typical cavity quality factor of $Q = 10^4$ and $\bar{B} = 8\text{T}$, can approach to the theoretical predictions of the KSVZ and DFSZ models, although it remains lower by approximately one to two orders of magnitude. However, as shown in Figure 3, under the same cryogenic conditions, even with a weak RF-excited magnetic field, e.g. $\tilde{B} \sim 10^{-12}\text{T}$, the upgraded scheme, by detecting the first-order electromagnetic response signal of axions in the low-frequency region, the achievable detection sensitivity can be approximately two orders of magnitude higher than that of conventional HTDs. Thus, it can reach the theoretically expected sensitivity. Continuously, if the excited magnetic field can be raised as $\tilde{B} = 10^{-6}\text{T}$, the proposed upgraded scheme can improve the detection sensitivity by three to four orders of magnitude, over conventional HTDs across the frequency range from MHz to 100 GHz. Such an achievable detection sensitivity could surpass the current level of the famous ADMX experiment. Probably, the most advantage of the upgraded scheme proposed here is its achievable detection is thermal noise insensitive and thus it can operate at even the room temperature.

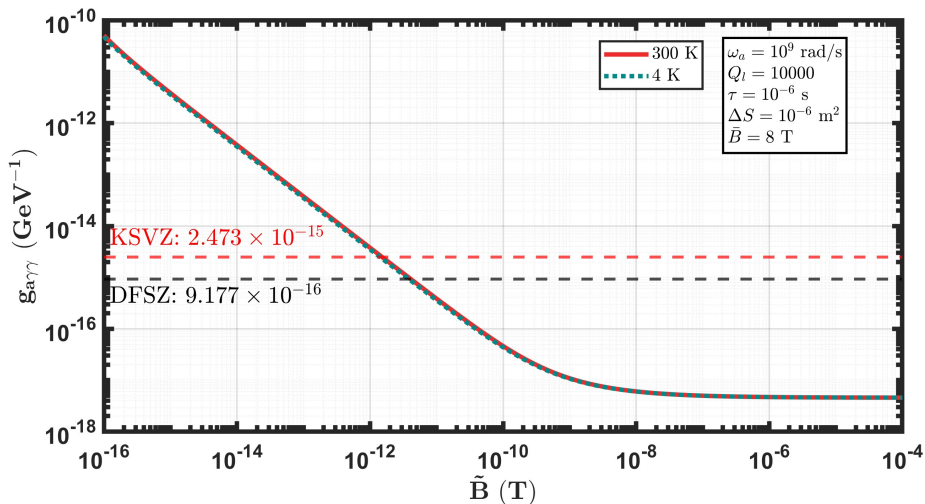


Figure 4. Relationship between the detection sensitivity of axion electromagnetic response based on the amplitude detection of first-order energy response signal and the amplitude of the excitation magnetic field \tilde{B}

Noted that the noise arising from the RF-field itself is related to its intensity. This im-

plies that, when the RF-field is used to enhance the achievable sensitivity for detecting the first-order electromagnetic response of axions, the stronger RF-field does not invariably lead to the higher achievable sensitivity. It can be seen from Figure 4 that, the achievable sensitivity for detecting the first-order electromagnetic response of axions gradually saturates with the increase of excitation magnetic field strength \tilde{B} . Specifically, for $\tilde{B} \geq 10^{-8}\text{T}$, the achievable detection sensitivity saturates at approximately $g_{a\gamma\gamma} \sim \times 10^{-18} \text{ GeV}^{-1}$. Nevertheless, with current microwave technology, it is not a difficult task to excite a mode magnetic field signal with an intensity on the order of $\tilde{B} = 10^{-6}\text{T}$ within a microwave cavity. Thus, at least theoretically, the proposed upgraded detection scheme is highly likely to improve the achievable detection sensitivity of conventional detection schemes by three to four orders of magnitude, thereby potentially exceeding the detectable sensitivity requirements predicted by the KSVZ and DFSZ models.

5 Conclusions and Discussions.

Given the existing HTD well-developed has not yet realized the desired EMR detection of the axions in RF- and microwave bands, here we propose a UHTD to significantly enhance the detection sensitivity. Specifically, we show that the detection of the existing HTD, which is biased only by a high SMF, is just the 2nd-order axion-photon energy signal; however, by additionally applying a transverse RF-excited magnetic field, the 1st EMR signal of the axions could be generated due to the 1st-order axion-photon interference energy signal. As a consequence, we argued that the achievable detection sensitivity of the proposed UHTD could be enhanced by $3 \sim 4$ orders of magnitude, compared with that obtained by using the usual HTDs, if the amplitude \tilde{B} of the applied RF-excited magnetic field is set as $1 \mu\text{T}$. As the amplitude of such a 1st-order electromagnetic response signal is detectable by using the usual IQ-mixer technique, the stronger RF-excited magnetic field leads to the higher detection sensitivity of the axion's electromagnetic response. Furthermore, the proposed UHTD could also be utilized to detect the axions with the lighter masses at the higher temperature, such as at 4 K and even at room temperature.

We now discuss the feasibility of the proposed UHTD. First, we argued that various robust filtering techniques could be utilized to implement the signal detection, although the strength of the generated 1st EMR signal is significantly weaker than that of the zeroth-order applied RF- or microwave signal (e.g., $P_{\text{rf}}^{(0)} = 1.19 \times 10^2 \text{W}$ for $\tilde{B} = 1 \mu\text{T}$). However, the latter one can be served, in principle, as an additional noise with the known frequency ω_B , while the frequency of the 1st EMRs of axion could be physically generated as $\omega_a \pm \omega_B$. Next, by increasing the cooling power and using the materials with sufficiently good thermal conductivity, the unwanted heating effect of the strong zeroth-order EM background noise could be avoided effectively. Additionally, although the analysis demonstrated here is just based on an idealized one-dimensional configuration, the proposal could be directly applied to the practical three-dimensional cylindrical cavity detectors.

Anyway, given the transverse RF-excited magnetic field technique has been widely applied in the usual magnetic resonance imaging field, it is particularly desirable to upgrade the existing HTD to significantly enhance the detection sensitivity of the axion field by

additionally applying the transverse RF-excited magnetic field for axion field detection is particularly desirable.

Acknowledgments

This work was partially supported by the National Natural Science Foundation of China (Grant No. P110325G02011), the National Natural Science Foundation of China (Grant No. 12505083), the Natural Science Foundation of Sichuan Province (Grant No. 2025ZNS-FSC0857), and the Natural Science Foundation of Sichuan Province (Grant No. 2025ZNS-FSC0858).

References

- [1] Y. Hochberg, Y. F. Kahn, R. K. Leane et al., *New approaches to dark matter detection*, *Nat. Rev. Phys.* **4**(2022)637.
- [2] P. A. R. Ade, N. Aghanim et al., *Planck 2015 results: XIII. Cosmological parameters*, *Astron. Astrophys.* **594**(2016)A13.
- [3] J. L. Feng, *Dark matter candidates from particle physics and methods of detection*, *Annu. Rev. Astron. Astrophys.* **48**(2010)495.
- [4] A. Ghosh, P. Konar, *Unveiling desert region in inert doublet model assisted by Peccei-Quinn symmetry*, *J. High Energ. Phys.* **2024**(2024)104.
- [5] E. Aprile and J. Aalbers, F. Agostini et al., *Dark matter search results from a one ton-year exposure of XENON1T*, *Phys. Rev. Lett.* **121**(2018)111302.
- [6] F. Chadha-Day, J. Ellis, D. J. E. Marsh, *Axion dark matter: What is it and why now?* *Sci. Adv.* **8**(2022)eabj3618.
- [7] P. W. Graham, I. G. Irastorza, S. K. Lamoreaux, A. Lindner, and K. A. van Bibber, *Experimental searches for the axion and axion-like particles*, *Annu. Rev. Nucl. Part. Sci.* **65**(2015)485.
- [8] Y. K. Semertzidis, S. Youn, *Axion dark matter: How to see it?*, *Sci. Adv.* **8**(2022)eabm9928.
- [9] D. G. Figueroa, M. Pieroni, A. Ricciardone, P. Simakachorn, *Cosmological Background Interpretation of Pulsar Timing Array Data*, *Phys. Rev. Lett.* **132**(2024)171002.
- [10] D. Budker, P. W. Graham, M. Ledbetter, S. Rajendran, A. O. Sushkov, *Proposal for a Cosmic Axion Spin Precession Experiment (CASPER)*, *Phys. Rev. X* **4**(2014)021030.
- [11] P. W. Graham and S. Rajendran, et al., *New observables for direct detection of axion dark matter*, *Phys. Rev. D* **88**(2013)035023.
- [12] C. B. Fu, X. P. Zhou, X. Chen, et al., *Limits on Axion Couplings from the First 80 Days of Data of the PandaX-II Experiment*, *Phys. Rev. Lett.* **119**(2017)181806.
- [13] H. Primakoff, *Photo-Production of Neutral Mesons in Nuclear Electric Fields and the Mean Life of the Neutral Meson*, *Phys. Rev.* **81**(1951)899.
- [14] T. Braine, R. Cervantes et al., *Extended Search for the Invisible Axion with the Axion Dark Matter Experiment*, *Phys. Rev. Lett.* **124**(2020)101303.

- [15] R. Khatiwada, D. Bowring et al., *Axion Dark Matter Experiment: Detailed design and operations*, *Rev. Sci. Instrum.* **92**(2021)124502.
- [16] S. DePanfilis, A. C. Melissinos, B. E. Moskowitz et al., *Limits on the abundance and coupling of cosmic axions at $4.5 < m_a < 5.0 \mu\text{eV}$* , *Phys. Rev. Lett.* **59**(1987)839.
- [17] I. Obata, T. Fujita, and Y. Michimura, *Optical Ring Cavity Search for Axion Dark Matter*, *Phys. Rev. Lett.* **121**(2018)161301.
- [18] D. J. E. Marsh, K. C. Fong, E. W. Lentz et al., *Proposal to Detect Dark Matter using Axionic Topological Antiferromagnets*, *Phys. Rev. Lett.* **123**(2019)121601.
- [19] S. A. Kenany, M. A. Anil et al., *Design and operational experience of a microwave cavity axion detector for the 20 – 100 μeV range*, *Nucl. Instrum. Methods Phys. Res. A* **854**(2017)11.
- [20] O. Kwon, D. Lee, W. Chung et al., *First Results from an Axion Haloscope at CAPP around 10.7 μeV* , *Phys. Rev. Lett.* **126**(2021)191802.
- [21] B. T. McAllister, G. Flower, E. N. Ivanov et al., *The ORGAN experiment: An axion haloscope above 15 GHz*, *Phys. Dark Universe* **18**(2017)67.
- [22] H. Chang, J. Y. Chang, Y. C. Chang et al., *First Results from the Taiwan Axion Search Experiment with a Haloscope at 19.6 μeV* , *Phys. Rev. Lett.* **129**(2022)111802.
- [23] P. Sikivie, *Axion dark matter*, *Nucl. Phys. B* **1003**(2024)116500.
- [24] A. Ghosh, P. Konar, *Precision Prediction of a democratic up-family philic KSVZ axion model at the LHC*, *Phys. Dark Universe* **47**(2025)101746.
- [25] A. Ghosh, P. Konar, R. Roshan, *Top-philic dark matter in a hybrid KSVZ axion framework*, *J. High Energy Phys.* **2022**(2022)167.
- [26] M. Dine, W. Fischler, M. Srednicki, *A simple solution to the strong CP problem with a harmless axion*, *Phys. Lett. B*, **104**(1981)199.
- [27] A. R. Zhitnitskii, *Weinberg's model of CP violation and T-odd correlations in weak decays*, *Sov. J. Nucl. Phys.* **31**(1980)4.
- [28] M. Sharifian, M. Zarei, M. Abdi et al., *Probing Virtual ALPs by Precision Phase Measurements: Time-Varying Magnetic Field Background*, *J. Cosmol. Astropart. Phys.* **2023**(2023)4.
- [29] R. Bush, S. Barke, H. Hollis et al., *Coherent detection of ultraweak electromagnetic fields Zachary*, *Phys. Rev. D* **99**(2019)022001.
- [30] Z. Omarov, J. Jeong, and Y. K. Semertzidis, *Speeding axion haloscope experiments using heterodyne-variance-based detection with a power meter*, *Phys. Rev. D* **107**(2023)103005.
- [31] H.B. Tran Tan, V.V. Flambaum, I.B. Samsonov et al., *Interference-assisted resonant detection of axions*, *Phys. Dark Universe* **24**(2019)100272.
- [32] J. W. Foster, N. L. Rodd, and B. R. Safdi, *Revealing the dark matter halo with axion direct detection*, *Phys. Rev. D* **97**(2018)123006.
- [33] R. F. Zheng, P. X. Wei, Q. L. Yang, *Exploring Quantum Aspects of Dark Matter Axions and Dark Photons Transitions within a Resonant Cavity*, arXiv:2410.12634.
- [34] X. Ma, Z. Cai, C. Zhuang et al., *Integrated microcavity electric field sensors using Pound-Drever-Hall detection*, *Nat. Commun.* **15**(2024)1386.

- [35] J. Yuan, W. Yang, M. Jing et al., *Quantum sensing of microwave electric fields based on Rydberg atoms*, *Rep. Prog. Phys.* **86**(2023)10.
- [36] J. Clarke, M. Hatridge, M. Mössle, *SQUID-detected magnetic resonance imaging in microtesla fields*, *Annu. Rev. Biomed. Eng.* **9**(2007)1.
- [37] X. He, Y. Wang, F. Jing and Y. Fan, *Weak Signal Detection Circuit Based on Dual-Phase Lock-in Amplification Technology*, *Academic Conference of China Instrument and Control Society (ACCIS)* **410**(2024).
- [38] Q. W. Zhang, W. Jeong , D. J. Kang, *Lock-in amplifiers as a platform for weak signal measurements: Development and applications*, *Curr. Appl. Phys.* **66**(2024)95.
- [39] Q. L. Yang, Y. Gao, Z. H. Peng, *Quantum dual-path interferometry scheme for axion dark matter searches*, *Nat. Commun. Phys.* **7**(2024)277.
- [40] D. He, J. Fan, X. Gao, et al., *Dark photon constraints from a 7.139 GHz cavity haloscope experiment*, *Phys. Rev. D* **110**(2024)L021101.